Available online at www.sciencedirect.com
SCIENCE DIRECT®
European Journal of Mechanics A/Solids 25 (2006) 1–12

Bucklewaves

Denzil G. Vaughn, John W. Hutchinson *

Division of Engineering and Applied Sciences, Harvard University, Cambridge, MA 02138, USA

Received 14 July 2005; accepted 27 September 2005

Available online 4 November 2005

Abstract

Motivated by a selection of results on the plastic buckling of column members within a sandwich plate core where one face of the sandwich is subject to an intense impulse, the problem addressed is one where lateral buckling takes place simultaneously as a compressive axial wave propagates down the member. The bucklewave problem is modeled as an infinitely long column (or wide plate) which is clamped against lateral deflection at the end where velocity is imposed and has a moving clamped condition coinciding with the front of the plastic compression wave. The model reveals that a column or plate suddenly compressed into the plastic range is dynamically stabilized against lateral buckling for lengths that are significantly longer than the corresponding length at which the member would buckle quasi-statically. This stabilization has significant implications for energy absorption under intense dynamic loading. The analysis method is benchmarked against a simpler, but mathematically analogous problem, for which closed form solutions are available: the dynamics of a guitar string lengthening at constant velocity.

Keywords: Columns; Plates; Dynamic buckling; Plastic buckling; Plastic waves; Energy absorption

1. Introduction

Dynamic buckling of columns and plates has been studied from various points of view for many years. We cite a limited selection of theoretical papers (Bell, 1988; Hayashi and Sano, 1972; Jones and Reis, 1980; Karagiozova and Jones, 1996; Kenny et al., 2002; Su et al., 1995) and experimental papers (Abrahamson and Goodier, 1966; Ari-Gur et al., 1982; Thornton and Yeung, 1990) which provide a background to the subject. In the theoretical work, all but a few recent studies have assumed the time required to produce the axial state of stress is sufficiently short compared to the time for lateral buckling deflections to evolve such that axial wave propagation can be decoupled from buckling by taking the axial stress to be established prior to buckling; coupled approaches are exceptional but they have been pursued by Anwen and Wenying (2003), Lepik (2001), Vaughn et al. (2005). Recent work by Vaughn et al. (2005) has shown that buckling cannot be decoupled from axial wave propagation when columns or plates are loaded at one end by high axial velocities, representative of those occurring in columns or plate webs in the cores of sandwich plates subject to blast loading. In what follows, to motivate the study in the paper, examples will be presented which clearly reveal that lateral buckling deflections develop simultaneously as the axial plastic wave propagates down the member when the velocity imposed on the end gives rise to stresses well into the plastic range. Buckling and axial wave propagation are intrinsically coupled in the form of a bucklewave. Lateral inertia stabilizes the member such that large compressive axial strains can develop simultaneously with the growth of buckling deflections.

* Corresponding author.
E-mail address: jhutchin@fas.harvard.edu (J.W. Hutchinson).

0997-7538/$ – see front matter
doi:10.1016/j.euromechsol.2005.09.003

Throughout the paper, the following notation for material properties will be used: elastic modulus, E; density, ρ; elastic wave speed, $c_0 = \sqrt{E/\rho}$; yield stress (positive in compression) σ_Y; and compressive yield strain, $\varepsilon_Y = \sigma_Y/E$. Without sacrifice of physical significance, the discussion and analysis will be simplified by restricting attention to materials with linear strain hardening having a tangent modulus, E_t, that is independent of strain. In uniaxial compression, with σ and ε positive in compression, the true stress-strain relation is $\varepsilon = \sigma/E$ for $\sigma \leqslant \sigma_Y$ and $\varepsilon = \varepsilon_Y + (\sigma - \sigma_Y)/E_t$ for $\sigma > \sigma_Y$. The plastic wave speed, whose significance will be detailed below, is given by (Taylor, 1958; Von Karman and Duwez, 1950; Vaughn et al., 2005)

$$c_p = \sqrt{\frac{E_t + \sigma}{\rho}} \cong \sqrt{\frac{E_t}{\rho}}. \tag{1}$$

The un-approximated expression applies with quantities defined in a finite strain context in terms of true stress and logarithmic strain. Finite strain aspects are not of primary importance in this paper; and because, usually, $\sigma/E_t \ll 1$, $c_p = \sqrt{E_t/\rho}$ will be used.

We begin by quoting some results for the axial propagation of plastic waves along a semi-infinite straight member ($0 \leqslant x < \infty$) initially at rest whose left end is abruptly moved at $t = 0$ with constant velocity V_0 so as to produce a uniaxial compression wave (Taylor, 1958; Von Karman and Duwez, 1950; Vaughn et al., 2005). If $V_0/c_0\varepsilon_Y < 1$, the ensuing strains are elastic. Of primary interest here are imposed velocities with $V_0/c_0\varepsilon_Y > 1$, such that strains exceed yield. Two distinct wave segments emerge. For $0 \leqslant x \leqslant c_p t$, the member moves with uniform velocity V_0 and is in a uniform state of stress and strain given to high accuracy by

$$\frac{\sigma}{\sigma_Y} = 1 + \sqrt{\frac{E_t}{E}}\left(\frac{V_0}{c_0\varepsilon_Y} - 1\right) \quad \text{and} \quad \frac{\varepsilon}{\varepsilon_Y} = 1 + \sqrt{\frac{E}{E_t}}\left(\frac{V_0}{c_0\varepsilon_Y} - 1\right). \tag{2}$$

In the transition region ahead of this uniform compressive state, the stress and strain decay monotonically (and sharply) with x, attaining initial yield values at the wave front at $x = c_0 t$. The front of the uniform compressive state propagates down the member with the plastic wave speed, c_p; it will be referred to as the plastic wave front in the sequel.

The dimensionless parameter characterizing the intensity of the compression wave is $V_0/c_0\varepsilon_Y$. With $E_t/E = 0.01$ as representative, axial strains of magnitude $\approx 100\varepsilon_Y$ are predicted by (2) if $V_0/c_0\varepsilon_Y \approx 10$. Many steel and aluminum alloys have $c_0\varepsilon_Y$ in the range from 5 to 20 m s^{-1}. Thus, typically, imposed velocities, V_0, greater than about 50 m s^{-1}, will generate compressive axial strains many times the yield strain.

These results provide the setting for the present study which is motivated by interest in the plastic buckling and energy absorption of columns and plates employed as core members in all-metal sandwich plates designed to withstand high intensity blast loads. An intense blast in either air or water imposes a sudden velocity typically in the range 50 to 200 m s^{-1} on the face sheet of the sandwich plate towards the blast (Fleck and Deshpande, 2004; Xue and Hutchinson, 2004). Core members experience this suddenly imposed velocity where they are attached to the impulsively loaded face sheet. The imposed velocity diminishes as the core is compressed, but the inertia of the face sheet towards the blast is substantial and, typically, the imposed velocity remains high for overall core crushing strains as large as 30% or even higher. Thus, for blast applications, the relevant dimensionless imposed velocity, $V_0/c_0\varepsilon_Y$, falls in the range where plastic waves will be initiated in the core members potentially generating relatively large compressive axial strains and associated plastic energy dissipation. The study herein reveals conditions under which the members can be expected to remain sufficiently straight, stabilized by lateral inertia, such that significantly enhanced energy absorption can indeed take place due to axial straining.

One of the early studies of dynamic buckling of suddenly compressed columns was performed by Abrahamson and Goodier (1966). Like many analyses that followed, their theoretical analysis decoupled plastic wave propagation and buckling by assuming the state of uniform stress was established along the entire member prior to the onset of lateral motion. Their experiments on aluminum rods fired against a massive anvil at velocities on the order of 100 m s^{-1} reveal that compressive axial strains as large as 20% can be achieved accompanied by only moderate buckling deflections (Fig. 1).

2. Selected numerical results illustrating coupled buckling and wave propagation

To illustrate the behavior experienced by a core column member oriented perpendicularly to the faces of a sandwich plate struck by a blast, we consider a unit cell model (see insert in Fig. 2) composed of solid circular column of length L and radius R clamped at each end to a rigid plate. The plates are constrained against rotation but are able to undergo free flight in the direction perpendicular to the faces. (An earlier related investigation by Vaughn et al. (2005) considered different conditions with the right end of the column fixed and the left end is subject to a uniform imposed velocity.) Each of the plates is assigned the same mass as the column, $m = \rho\pi R^2 L$, representing a sandwich plate with one third of its total mass in the core, which is not untypical for all-metal sandwich plates designed against impulsive loads. More extensive investigation of the preferred proportion of metal

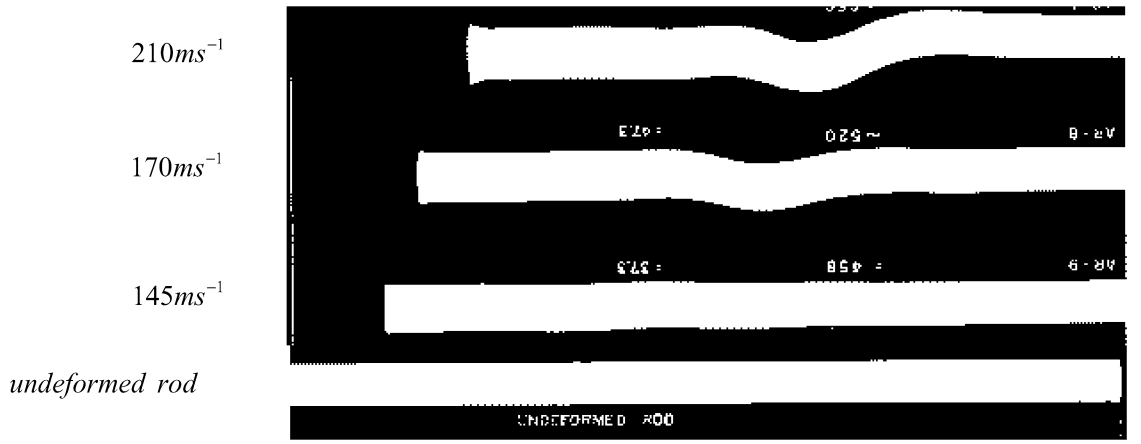

Fig. 1. Aluminum rods impacting a massive anvil at the velocities ranging from 145 to 210 m s^{-1} showing large axial compression and buckling deformations from Abrahamson and Goodier (1966).

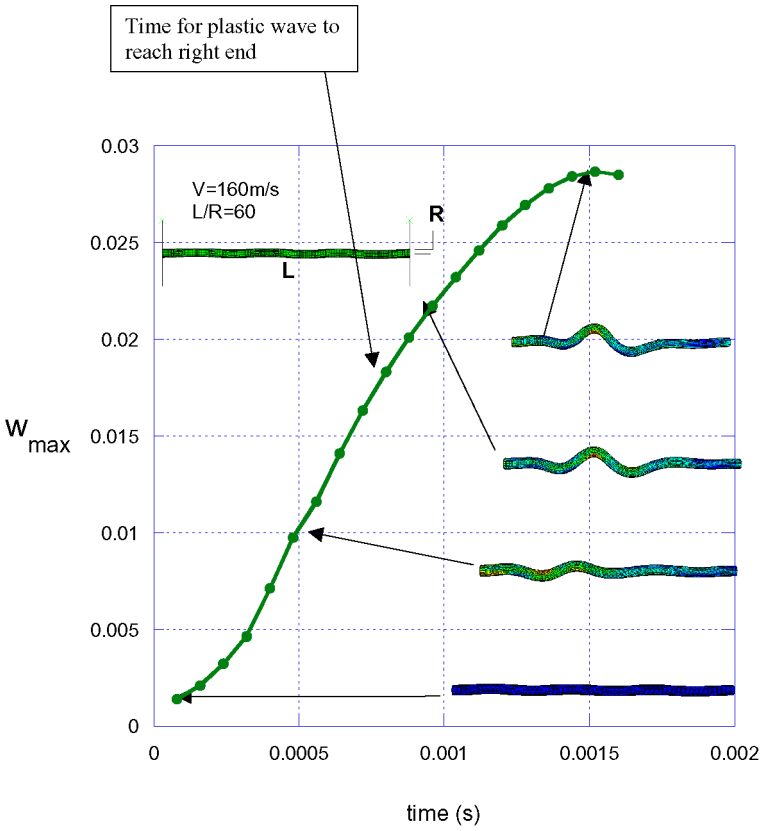

Fig. 2. Development of lateral buckling deflection ($w_{\max}$ in m) in free-flight model pictured in insert for $V_0 = 160$ m s^{-1}, $L/R = 60$, $L = 0.567$ m and imperfection amplitude $\delta_R/R = 1/4$ and mode $n = 6$. The time at which the plastic wave front reaches the right end of the column is indicated. Material properties are cited in the text.

in the core and face sheets has been given elsewhere (Fleck and Deshpande, 2004; Hutchinson and Xue, 2005). At $t = 0$, the column and the plate on the right end are at rest, but the plate at the left end is abruptly set in motion with initial velocity V_0 towards the plate at the right end. The column material is taken to be representative of a stainless steels being considered for such applications with $E = 190$ GPa, $\rho = 7920$ kg m^{-3} and $\sigma_Y = 400$ MPa, and $E_t = 2.4$ GPa; thus, $c_0 = 4898$ m s^{-1},

$c_p = 550\ \mathrm{m\,s^{-1}}$ and $\varepsilon_Y = 0.0021$. Material rate dependence is neglected. In the numerical examples presented, the column length is fixed at $L = 0.567$ m; the radius is varied to generate results for various values of the slenderness ratio, R/L.

The initial kinetic energy imparted to the model is $mV_0^2/2$. Apart from relatively small elastic vibratory motion, the entire unit cell moves with a common velocity after the column is compressed. Conservation of momentum gives the common velocity as $V_0/3$ and the associated kinetic energy of the unit cell as $mV_0^2/6$. Assume the kinetic energy deficit, $mV_0^2/3$, is dissipated entirely in plastic deformation of the column during the stage the unit cell attains the common velocity (the numerical simulations verify this). Further, to obtain a simple approximate relation, assume the column remains straight and that the compressive plastic strain, ε^P, is uniformly distributed along the full length of the column. Then, equating $mV_0^2/3$ to the plastic deformation in the column, one obtains

$$\frac{\varepsilon^P}{\varepsilon_Y} + \frac{1}{2}\frac{E_t}{E}\left(\frac{\varepsilon^P}{\varepsilon_Y}\right)^2 = \frac{1}{3}\left(\frac{V_0}{c_0\varepsilon_Y}\right)^2. \tag{3}$$

As will be seen, this equation provides a useful reference to understand detailed numerical results for the model.

The numerical simulations have been carried out using the finite strain version of ABAQUS Explicit (2001). The column is fully meshed using three-dimensional hexahedral elements. At both ends it is rigidly attached to the face plates which are comprised of rigid elements that cannot deform. The mesh density was increased beyond the level reported here without an appreciable change in the results. Initial imperfections in the form of slight lateral waviness play a critical role in the response, and for each slenderness ratio an entire set of geometric imperfections was generated by employing ABAQUS to compute the buckling eigenfunctions for the quasi-static problem of the perfect elastic column subject to a compressive axial force. The initial imperfections were taken to be proportional to these eigenfunctions. Away from the ends, the lateral deflection of the eigenfunction is approximately sinusoidal in form (with zero deflection and slope at the ends). The number of local maxima and minima of the initial deflection, n, will be used to identify the imperfection, and the magnitude of the maxima, δ_I, will be referred to as the imperfection amplitude. The mesh used to generate the imperfections is the same as that used in the dynamic computations, permitting the nodal locations of the imperfect column to be transported directly into the dynamic code.

An example which illustrates that the buckling deflection develops simultaneously with the propagation of the compression wave down the column is presented in Fig. 2. The maximum lateral buckling deflection, w_{max}, is plotted as a function of time, including snap shots of the column at four stages of deformation. For reference, the time (7.8×10^{-4} s) that the plastic wave front reaches the right end is noted. The initial imperfection in this example was chosen having $\delta_I/R = 1/4$ with $n = 6$, corresponding to an imperfection wavelength ($L_I \approx L/3$) that is near critical. It is apparent from Fig. 2 that buckling is well underway by the time the compression wave is just half-way down the column, and the buckling deflection has mainly formed by the time the compression wave reaches the right end of the column.

Further evidence for the coupling between the axial plastic wave and lateral buckling can be seen in Fig. 3 where the axial compressive strain, ε_{33}, at many points across one transverse section through the beam (at $x = 0.47L$) is plotted as a function of time. The times of arrival of both the initial wave front (x/c_0) and the plastic wave front (x/c_p) are noted on Fig. 3. Yielding occurs with the arrival of the initial wave front, but the sharp rise in strain occurs only with the arrival of the plastic wave front. This sharp rise of strain in time is associated with a steep fall off in space of stress and strain in the transition region ahead of the plastic wave front. The strain at the midsection is essentially constant after the plastic wave front has passed, consistent with the existence of a uniform state behind the front when there is no initial imperfection. The divergence of the strains in Fig. 3 is associated with the growth of the buckling deflection. Prior to arrival of the plastic wave front the buckling deflection is very small. However, it grows rapidly after arrival of the plastic wave front as evidenced by the diverging strain magnitudes across the cross-section. Somewhat later (at $t \cong 0.00065$ s but well before the plastic wave front reaches the right end), the strains cease to change implying that the buckling deflection is fully developed at this location.

Define the overall strain of the column as $\bar{\varepsilon} = \Delta/L$ where Δ is the permanent shortening of the distance between its ends. Fig. 4 presents the final overall strain as a function of the slenderness ratio for simulations with $V_0 = 160\ \mathrm{m\,s^{-1}}$ for columns each having $\delta_I/R = 1/4$ with $n = 6$. Snap shots of the final deformed state are shown for four values of slenderness. One immediately notes that the more stocky columns develop much smaller buckling deflections than their slender counterparts, but even the most slender columns have been significantly stabilized by lateral inertia. The overall strain in the more stocky columns ($\approx 11\%$) is roughly $60\varepsilon_Y$ and is almost entirely due to axial compression. For the relatively slender column discussed in connection with Fig. 2 with $L/R = 60$, more than three quarters of the overall strain of 13.5% is due to axial compression and less than one quarter is a result of buckling. Although not shown, plastic dissipation was computed for each column in Fig. 4 giving $mV_0^2/3$ to within a few percent; the missing energy is associated with persistent elastic vibrations of the unit cell.

The wavelength of the initial imperfection, $L_I \approx 2L/n$, is an important parameter in dynamic buckling, as illustrated by the results in Fig. 5. The final overall strain for the unit cell having a slender column with $L/R = 80$ and set in motion with various initial velocities, V_0, is plotted in Fig. 5 for the full range of relevant wave numbers, n, all with $\delta_I/R = 1/4$. For this slenderness ratio, the initial imperfection that produces the largest buckling deflection (and, thus, the largest end shortening) has $n \approx 6$. At the largest values of $V_0/c_0\varepsilon_Y$ plotted, an imperfection in the critical mode results in an end shortening that is

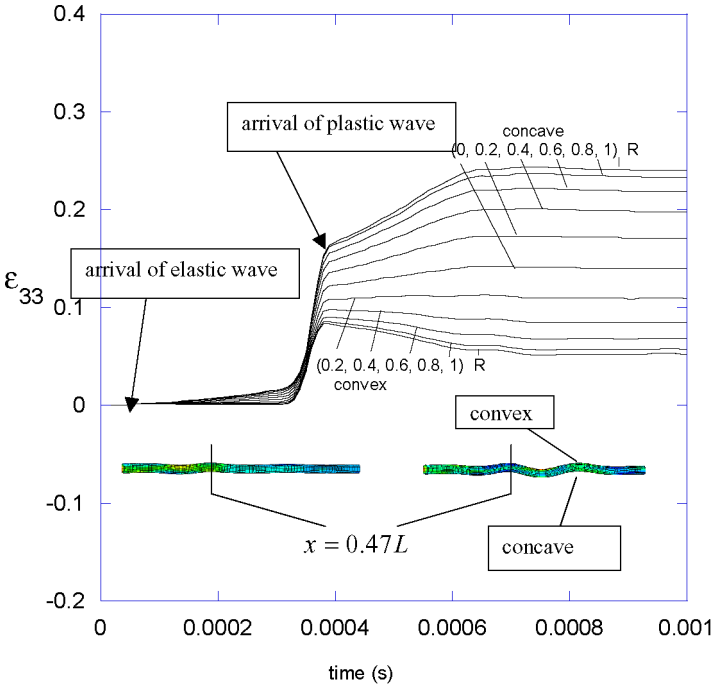

Fig. 3. Axial strain distribution across the column cross-section at $x = 0.47L$ in the free-flight model as a function of time ($V_0 = 160\ \mathrm{m\,s^{-1}}$, $L/R = 60$, $L = 0.567$ m, $\delta_1/R = 1/10$ and $n = 6$). The times at which the elastic and plastic wave fronts reach this point are indicated. The jump in plastic strain occurs when the plastic wave front passes the point. As buckling develops, plastic compressive loading occurs at all times on the concave side of the buckle, but elastic unloading and immediate reloading in tension on the convex side.

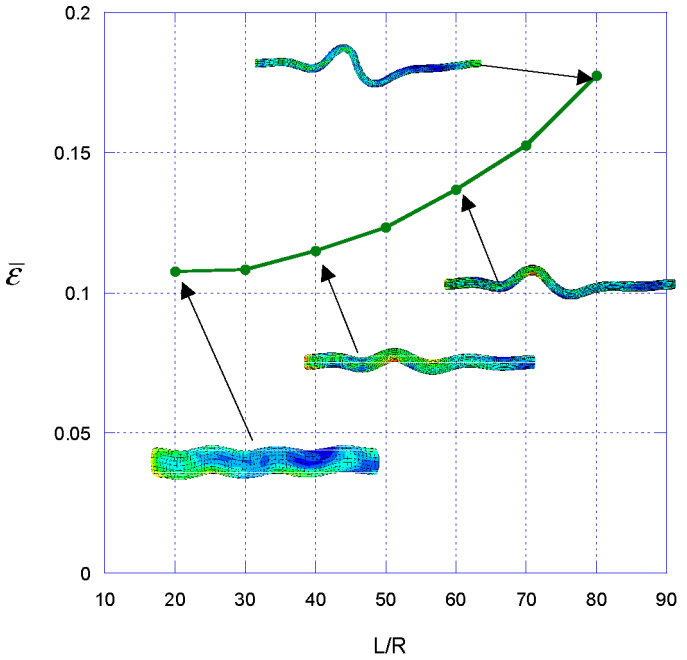

Fig. 4. Final overall strain and buckle shapes of the free-flight model as a function of the slenderness ratio for $V_0 = 160\ \mathrm{m\,s^{-1}}$, $L/R = 60$, $L = 0.567$ m, $\delta_1/R = 1/4$ and $n = 6$. Material properties are cited in the text. The overall strain 0.11 for $L/R = 20$ and 30 is essentially that for a column that undergoes no buckling.

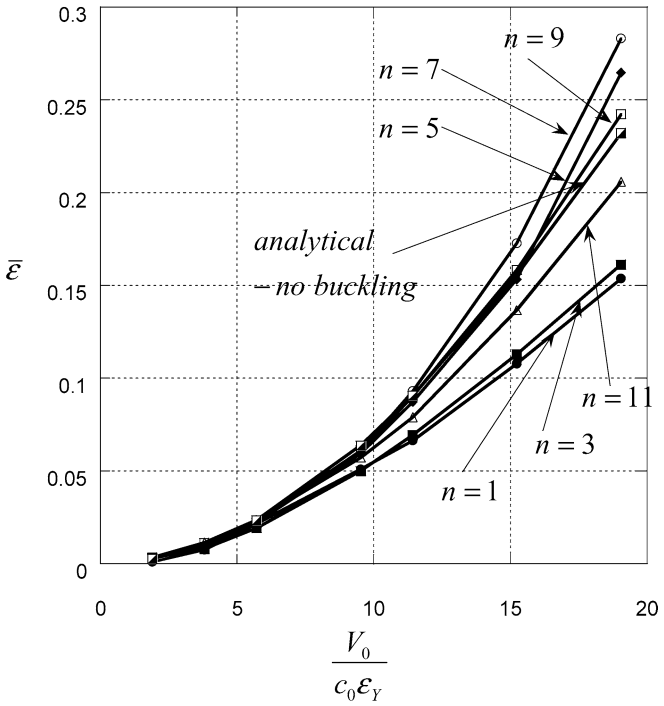

Fig. 5. Final overall strain of the free-flight model for the full range of initial imperfection mode shapes, n, for $V_0 = 160\ \mathrm{m\,s^{-1}}$, $L/R = 80$, $L = 0.567$ m, and $\delta_I/R = 1/4$. Included in the figure is the result (3) determined under the assumption that no buckling occurs and the plastic strain is uniformly distributed.

twice that predicted for columns whose initial imperfections are so far away from being critical (e.g. $n = 1$ or $n = 11$) that they undergo very little buckling. The simple result (3) derived under the assumption of no buckling captures the general trend of the dependence of the overall strain on $V_0/c_0\varepsilon_Y$, but it is not strictly correct even when there is no buckling since the axial strain is not uniformly distributed along the member. Further insight into the critical imperfection wavelength emerges from the bucklewave model.

3. The bucklewave model

As depicted in Fig. 6, the lateral deflection of the column, $w(x,t)$, in the bucklewave is modeled by an infinitely long beam that is clamped both at the left end and at the moving right end, $x_R = \sqrt{E_t/\rho}\,t$: i.e.

$$w(0,t) = w_{,x}(0,t) = 0, \quad \text{and} \quad w(x_R,t) = w_{,x}(x_R,t) = 0. \tag{4}$$

The right clamp moves at constant velocity along the beam, coinciding with the front of the region of uniform compressive stress, σ, associated with the axial wave propagating along the column.

The primary interest here is in plastic waves, but it can be noted in passing that the model is also applicable in the elastic range, and the rationale for the moving end condition for elastic behavior is argued first. If $V_0/c_0\varepsilon_Y < 1$, the compression wave is elastic ($E_t = E$) and a uniform stress $\sigma = EV_0/c_0$ exists throughout the region behind the wave front at $x_R = \sqrt{E/\rho}\,t$. For $x > x_R$ the beam is undisturbed. Thus, zero deflection and slope at $x = x_R$ is necessarily imposed on the lengthening beam.

The argument for taking clamped conditions at $x_R = c_p t$ when $V_0/c_0\varepsilon_Y > 1$ is less clear because of the existence of the transition region ahead of x_R where yielding occurs. Nevertheless, the numerical solutions of the previous section reveal both a sharp fall off in axial stress and strain with distance ahead of x_R and very small lateral deflections in the transition region, consistent with the approximation of the beam being clamped at x_R. Another feature in Fig. 3 relevant to bucklewave modeling is the elastic unloading and subsequent plastic reloading with tensile strain increments that occur on the convex side of the cross-section due to bending. The switch from compressive loading to tensile loading occurs over a very short period of time, just after the arrival of the plastic wave front, because the plastic strains are large compared to ε_Y. In the model, the short elastic unloading period is ignored and the tangent modulus, E_t, is taken to govern the bending stiffness everywhere in the beam behind the plastic wave front. This approximation is consistent with the fact that the strains are large compared to ε_Y. Thus, the model

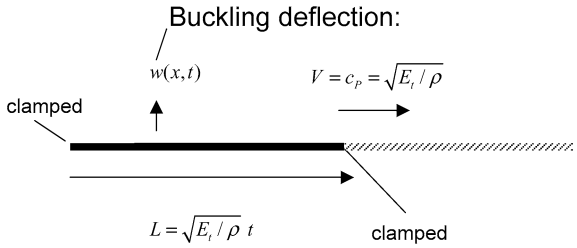

Fig. 6. The bucklewave model for the lateral buckling deflection.

is based on the notion that the beam is most susceptible to buckling in the region of high compressive stress and low bending stiffness on $0 \leqslant x \leqslant x_{\mathrm{R}}$. The moving clamp condition at x_{R} overestimates the constraint of the beam segment ahead of x_{R}, but it appears to be a good modeling approximation based on the numerical simulations.

With I and A as the moment of inertia and cross-sectional area of the beam the equation governing the lateral deflection is

$$E_{\mathrm{t}} I w_{,xxxx} + \sigma(w_{,xx} + w_{0,xx}) = -\rho A w_{,tt} \quad \text{on } 0 \leqslant x \leqslant x_{\mathrm{R}} = \sqrt{E_{\mathrm{t}}/\rho}\, t \tag{5}$$

where $w_0(x)$ is the initial imperfection. The equation applies to the elastic case with E_{t} replaced by E. Eq. (5) is often referred to as the beam-column equation. Von Karman plate theory for a wide plate undergoing one-dimensional deflections reduces to (5) if $I = h^3/12(1-\nu^2)$ and $A = h$ where h is the plate thickness and ν is Poisson's ratio.

4. Carrier's guitar string problem

The bucklewave problem cannot be solved in closed form. An analogous, lower order problem for the dynamics of a guitar string fixed at $x = 0$ with right end that lengthens at constant velocity has closed form solutions (Carrier, 1949), and, moreover, provides a benchmark for validating the numerical method employed to solve the bucklewave problem. The lateral deflection, $w(x,t)$, of the string satisfies the wave equation, $w_{,xx} - c_0^{-2} w_{,tt} = 0$, subject to $w(0,t) = 0$ and $w(x_{\mathrm{R}}, t) = 0$. The prescribed lengthening rate is c with $x_{\mathrm{R}} = ct$; attention is restricted to subsonic lengthening with $\lambda \equiv c/c_0 < 1$.

The analytical solution which follows makes use of the dimensionless variable, $\xi = x/ct$, with the fixed range, $0 \leqslant \xi \leqslant 1$. With $\tau = \ln(t)$, Carrier showed that separable solutions exist with

$$w(x,t) = \mathrm{Re}\big(Y(\xi)(\lambda^{-2} - \xi^2)^{(\mathrm{i}\omega - 1)/2}\, \mathrm{e}^{\mathrm{i}\omega\tau}\big) \tag{6}$$

where $\mathrm{i} = \sqrt{-1}$ and the eigenvalue problem for (Y, ω) is

$$\frac{\mathrm{d}^2 Y}{\mathrm{d}^2 \xi} - \frac{\lambda^2(1+\omega^2)}{(1-\lambda^2\xi^2)^2} Y = 0, \qquad Y(0) = Y(1) = 0. \tag{7}$$

The eigenvalue problem must be solved numerically, but standard methods apply.

An example of a solution generated by the above recipe is shown in Fig. 7 for a lengthening rate set at one half of the wave speed, $\lambda = 1/2$. The deflection of the string is plotted as a function of x/x_0 for several values of t/t_0 corresponding to roughly one full oscillation period in which the length of the string more than doubles. Here, t_0 is introduced as reference time and $x_0 = ct_0$. This solution, and others, was used to validate the numerical solution method employed for the buckle wave problem, as will be described in the next section.

5. Solution of the bucklewave problem

5.1. Reduction to a system of ordinary differential equations

Eq. (5) is transformed using a variable similar to that employed in the guitar string problem: $\xi = x/x_{\mathrm{R}} = x/c_{\mathrm{p}}t$, with fixed range $0 \leqslant \xi \leqslant 1$. With $w(x,t) = f(\xi,\tau)$ and dimensionless time, $\tau = c_{\mathrm{p}}t/r$, where $r = \sqrt{I/A}$ is the radius of gyration of the cross-section, (5) becomes

$$\tau^2 f_{,\tau\tau} - 2\xi\tau f_{,x\tau} + (\xi^2 f_{,\xi})_{,\xi} + S f_{,\xi\xi} + \tau^{-2} f_{,\xi\xi\xi\xi} = -S(r\tau)^2 w_{0,xx} \tag{8}$$

where $S = \sigma/E_{\mathrm{t}}$. The imperfection adopted in the present study is

$$w_0(x) = \frac{\delta_{\mathrm{I}}}{2}\left(1 - \cos\left(\frac{2\pi x}{L_{\mathrm{I}}}\right)\right) \tag{9}$$

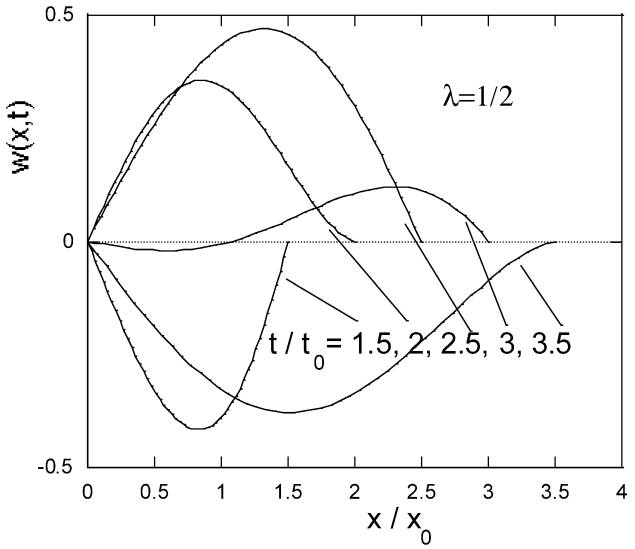

Fig. 7. An example of the motion of a guitar string where the left end ($x = 0$) is fixed and the right end ($x = ct$) moves at constant velocity. The example with $\lambda = c/c_0 = 1/2$ shows roughly one full oscillation period during which the length of the string has more than doubled.

where L_{I} will be referred to as the imperfection wavelength.

Solutions to (8) are sought in the form of an eigenfunction expansion

$$f(\xi,\tau) = \sum_{n=1}^{N} a_n(\tau) u_n(\xi). \tag{10}$$

The eigenfunctions and associated eigenvalues, $\{u_n, \lambda_n\}$, are generated from the problem

$$\frac{\mathrm{d}^4 u_n}{\mathrm{d}^4 \xi} - \lambda_n^4 u_n = 0, \quad \text{with } u_n(0) = \frac{\mathrm{d}u_n(0)}{\mathrm{d}\xi} = u_n(1) = \frac{\mathrm{d}u_n(1)}{\mathrm{d}\xi} = 0. \tag{11}$$

Analytical expressions for the eigenfunctions and the eigenvalue equation are readily obtained. The latter is used to generate numerical values for the eigenvalues. Details need not be included here. The eigenfunctions are orthogonal and each satisfies the clamped conditions at the ends of the interval.

The equations governing the $a_n(\tau)$ are obtained by substitution of (10) into (8) and adoption of a Galerkin procedure enforcing the requirement, $\int_0^1 \{\} u_m \,\mathrm{d}\xi = 0$ for $m = 1, N$ where $\{\cdot\}$ denotes all the terms in (8). The result is

$$\begin{aligned} &\ddot{a}_m - 2\tau^{-1} \sum_{n=1}^{N} D_{mn}^{(1)} \dot{a}_n + \sum_{n=1}^{N} [-D_{mn}^{(2)} - S D_{mn}^{(3)}] \tau^{-2} a_n + \tau^{-4} \lambda_m^4 a_m \\ &\quad = -\frac{2\pi^2 S (r/L_{\mathrm{I}})^2 \delta_{\mathrm{I}}}{c_m} \int_0^1 \cos\left(\frac{2\pi\tau r}{L_{\mathrm{I}}}\xi\right) u_m(\xi)\,\mathrm{d}\xi \equiv R_m(\tau), \quad m = 1, N, \end{aligned} \tag{12}$$

where

$$c_m = \int_0^1 u_m^2 \,\mathrm{d}\xi, \quad D_{mn}^{(1)} = \frac{\int_0^1 \xi u_n' u_m \,\mathrm{d}\xi}{c_m}, \quad D_{mn}^{(2)} = \frac{\int_0^1 \xi^2 u_n' u_m' \,\mathrm{d}\xi}{c_m}, \quad D_{mn}^{(3)} = \frac{\int_0^1 u_n' u_m' \,\mathrm{d}\xi}{c_m}.$$

This system of coupled ordinary differential equations can be expressed in vector-matrix form as

$$\ddot{a} = 2\tau^{-1} D^{(1)} \dot{a} + \tau^{-2} (D^{(2)} + S D^{(3)}) a - \tau^{-4} D^{(4)} a + R \tag{13}$$

where

$$a = \begin{bmatrix} a_1 \\ \bullet \\ a_N \end{bmatrix}, \quad R = \begin{bmatrix} R_1 \\ \bullet \\ R_N \end{bmatrix}, \quad D^{(4)} = \begin{bmatrix} \lambda_1^4 & & \\ & \bullet & \\ & & \lambda_N^4 \end{bmatrix}.$$

Initial conditions require special consideration because the beam has zero length at $\tau = 0$. For small τ, the contribution in (12) from the inhomogeneous term due to the imperfection (9) is $R_m(\tau) = -(2\pi^2 S(r/L_\mathrm{I})^2 \delta_\mathrm{I}/c_m) \int_0^1 u_m(\xi)\,\mathrm{d}\xi$. Careful examination of the system of Eqs. (12) reveals that to lowest order in τ, $\tau^{-4}\lambda_m^4 a_m$ and $R_m(\tau)$ are dominant and they must balance one another such that for sufficiently small τ,

$$a_m = -\tau^4\big(2\pi^2 S(r/L_\mathrm{I})^2 \delta_\mathrm{I}/\lambda_m^4 c_m\big) \int_0^1 u_m(\xi)\,\mathrm{d}\xi, \quad m = 1, N. \tag{14}$$

These provide the "initial" conditions for the system of differential equations.

The system of Eqs. (12) is linear in the a_m, and these amplitudes are proportional to the imperfection amplitude, δ_I. Only two dimensionless parameters, S and L_I/r, appear in (12) and (14), in addition to the dimensionless time, $\tau = c_\mathrm{p} t/r$. For purposes of interpreting the solutions, alternative length and time scales are introduced. Let L_C be the length of a beam (or wide plate), clamped at both ends, at the onset of quasi-static buckling when compressed into the plastic range by stress σ:

$$L_\mathrm{C} = 2\pi r\sqrt{E_\mathrm{t}/\sigma} = 2\pi r/\sqrt{S}. \tag{15}$$

Let t_C be the time for a plastic wave front to propagate the distance L_C:

$$t_\mathrm{C} = L_\mathrm{C}/c_\mathrm{p}. \tag{16}$$

With these definitions,

$$\frac{L_\mathrm{I}}{r} = \frac{2\pi}{\sqrt{S}}\frac{L_\mathrm{I}}{L_\mathrm{C}} \quad \text{and} \quad \tau = \frac{2\pi}{\sqrt{S}}\frac{t}{t_\mathrm{C}}. \tag{17}$$

In presenting results below, we will use S, $L_\mathrm{I}/L_\mathrm{C}$ and t/t_C.

5.2. The analytical form solution for the one mode approximation, $N = 1$

The solution for a one-mode approximation gives analytical insight and provides another check on the numerical solution because it can be expressed in analytical form, although it is unable to capture shape evolution of the deflection. With $N = 1$, (12) for $a_1(\tau)$ becomes

$$\ddot{a}_1 + \tau^{-1}\dot{a}_1 + \big[\tau^{-4}\lambda_1^4 - \tau^{-2}(\alpha + S\beta)\big]a_1 = R_1(\tau) \tag{18}$$

where $\lambda_1 = 4.730$, $\alpha = c_1^{-1}\int_0^1 \xi^2 u_1'^2\,\mathrm{d}\xi = 4.052$ and $\beta = c_1^{-1}\int_0^1 u_1'^2\,\mathrm{d}\xi = 12.303$. The homogeneous solution to (18) can be expressed as linear combinations of the Bessel functions $J_\nu(\lambda_1^2/\tau)$ and $Y_\nu(\lambda_1^2/\tau)$, where $\nu^2 = \alpha + S\beta$. The "variation of parameters" solution to (18) satisfying the starting condition (14) is

$$a_1(\tau) = \frac{\pi}{2}\left[J_\nu\left(\frac{\lambda_1^2}{\tau}\right)\int_0^\tau t Y_\nu\left(\frac{\lambda_1^2}{t}\right)R_1(t)\,\mathrm{d}t - Y_\nu\left(\frac{\lambda_1^2}{\tau}\right)\int_0^\tau t J_\nu\left(\frac{\lambda_1^2}{t}\right)R_1(t)\,\mathrm{d}t\right]. \tag{19}$$

The dependence of the maximum deflection $w_\mathrm{max} = (a_1 u_1)_\mathrm{max}$ as a function of t/t_C for various S has been computed from (19) and is plotted in Fig. 8. An unbounded response as t/t_C increases arises due to the logarithmic behavior of Y_ν as its argument approaches zero. As will be discussed in connection with the full numerical results, the ranges of S and t/t_C in Fig. 8 are those relevant to the plastic bucklewave problem. The trends seen in Fig. 8 are qualitatively correct, although the one-mode solution is a poor approximation for reasons discussed below.

5.3. Numerical solutions for multiple modes

To validate the approach laid out above for the bucklewave problem, the same transformation of variables, eigenfunction expansion and Galerkin procedure were applied to the guitar string problem. In this case, the eigenfunctions are $\{\sin(n\pi\xi)\}$, which satisfy the single boundary condition at each end of the interval. The resulting system of equations is analogous to (12) and (13) but without the inhomogeneous term. A numerical solution of the system of ordinary differential equations (13) was obtained using standard methods (a Runge–Kutta–Verner method), and the string deflection was computed from (10) and compared with responses such as those in Fig. 7. Initial conditions on a_n and $\dot{a}_n$ were obtained by fitting $w(x,t)$ and $\dot{w}(x,t)$ to the expansion at a starting time (e.g. $t/t_0 = 3/2$ in Fig. 7), and the deflection was computed at subsequent times. In this manner, it was found that the exact results in Fig. 7 could be reproduced to high accuracy (within a small fraction of a percent) over the time range shown for expansions with $N = 7$.

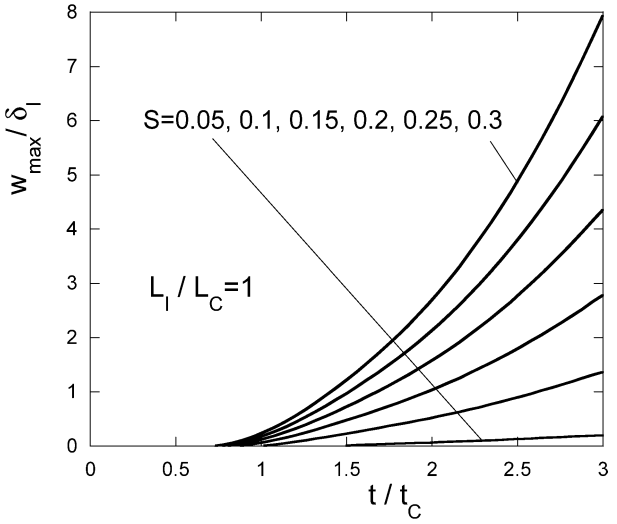

Fig. 8. Growth of the maximum lateral deflection of the bucklewave for the one-mode approximation ($N = 1$) with $L_1/L_C = 1$.

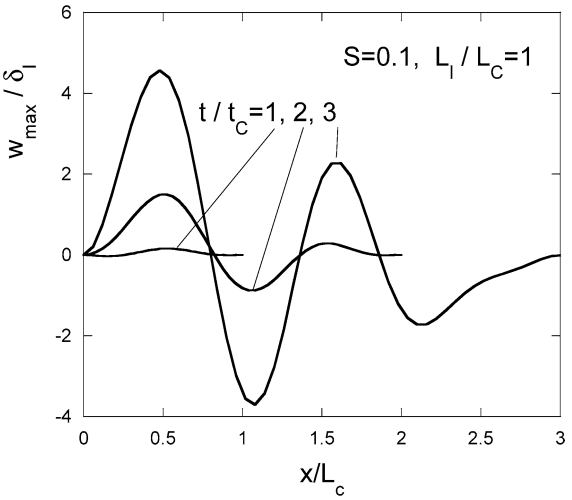

Fig. 9. Snapshots of the lateral buckling deflection of the bucklewave at three times with $S = \sigma/E_t = 0.1$, $L_1/L_C = 1$ and $N = 7$.

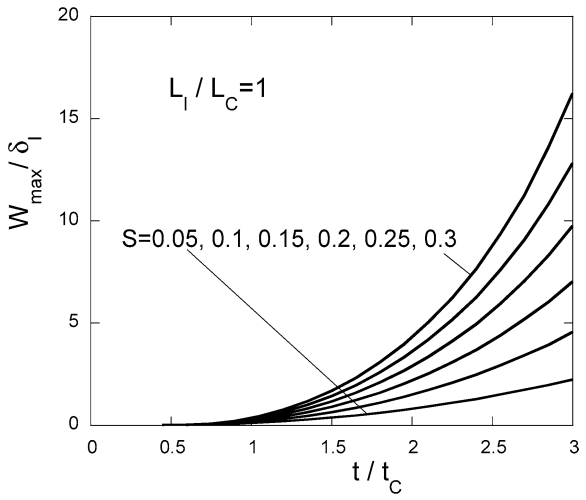

Fig. 10. Growth of the maximum lateral deflection of the bucklewave at various $S = \sigma/E_t$ with $L_1/L_C = 1$ and $N = 7$.

The numerical procedure for generating bucklewaves is similar to that described above except that initial conditions on a_n and $\dot{a}_n$ are determined from (14) by taking a very small starting time, $t/t_C \approx 0.01$. The numerical solution was insensitive to the choice of staring time over a fairly wide range of values. Seven-mode expansions ($N = 7$) were found to be adequate over the time range of interest. The exact one-mode solution (19) was used to check the numerical program for $N = 1$.

An illustration of the growth of the beam deflection as the compression wave propagates along the beam is shown in Fig. 9 for the case $L_1/L_C = 1$ and $S = \sigma/E_t = 0.1$. The deflection is shown at three times when the plastic wave front has traveled the distance L_C, $2L_C$ and $3L_C$, respectively, where L_C has been defined in (15) as the length at which a clamped beam buckles quasi-statically under the same compressive stress. Very little deflection growth has occurred at the time the front attains L_C, and even when the front has reached $3L_C$ the maximum deflection is less than five times the initial imperfection amplitude. At $t/t_C = 3$ the maximum deflection occurs at $x \cong L_C/2$, but the magnitude of the deflection at $x \cong L_C$ is growing more rapidly at this time and subsequently it becomes larger than the deflection at $x \cong L_C/2$. A notable feature of the solution is the fact that the locations of the local peaks are essentially frozen in space even though the length of the deforming beam is increasing. The one-mode solution cannot capture this feature as its peak coincides with the maximum of $u_1(\xi)$ which always lies midway along the expanding uniformly stressed region.

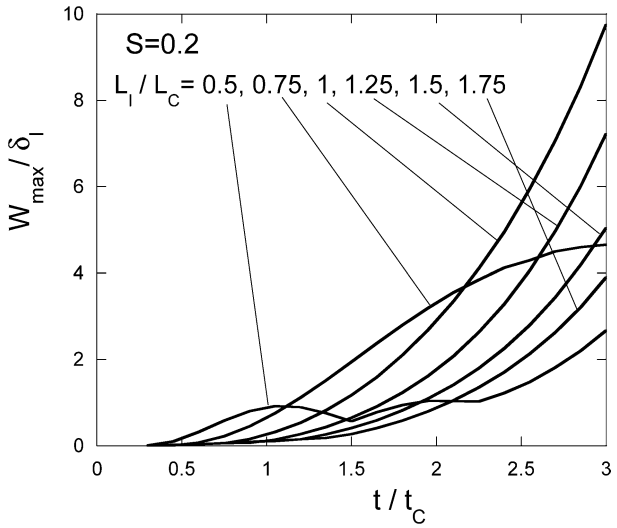

Fig. 11. Growth of the maximum lateral deflection of the bucklewave with various imperfection wavelengths, L_I/L_C, with $S = \sigma/E_t = 0.2$ and $N = 7$.

The magnitude of the maximum deflection is plotted as a function of time in Fig. 10 for a wide range of S, again with $L_I/L_C = 1$. The range of S is consistent with the range of interest for $V_0/c_0\varepsilon_Y$ noted in connection with (2). Note that, by (15), L_C depends on S, so that both L_I and t_C decrease as S is increased. Increasing S results in more rapid growth of the bucking deflection, as would be expected. Nevertheless, even at the largest values of S in Fig. 10, the maximum buckling deflection has only grown to $\approx 15\delta_I$ by the time the plastic wave front has reached $3L_C$. For beams with small initial imperfections, this is a modest buckling deflection. The main conclusion to be drawn from Figs. 9 and 10 is that lateral inertial stabilizes the beam such that it remains nearly straight even when the axial plastic wave front has engulfed three or more times the length of beam associated with quasi-static buckling. As emphasized in connection with (2), the plastic strains associated with the axial compression wave are large when $V_0/c_0\varepsilon_Y > 5$. The important consequence for applications is that the significant energy dissipation associated with the axial compression wave can be expected to occur over lengths of $3L_C$ or even longer before buckling alleviates the load on the column.

The role of the imperfection wavelength, L_I, is seen in Fig. 11 where the growth of the maximum deflection is plotted for various L_I/L_C in each case for $S = 0.2$. At small times, the imperfections with the shortest wavelengths grow the most rapidly since the length of the beam engulfed by the plastic wave is still small. At larger times ($t/t_C \approx 2$), the deflection having imperfection wavelength $L_I/L_C = 1$ becomes the largest and, at least until $t/t_C = 3$, this dominance persists. At even longer times, imperfections with longer wavelengths may give rise to larger deflections. Thus, for this example, when the buckling deflection develops during the period $t/t_C = 3$, the critical imperfection has a wavelength roughly equal to the quasi-static mode length L_C. Calculations with other values of S indicate that imperfection wavelengths longer than L_C can give rise to larger buckling deflections when the column is much longer than L_C and t is much greater than t_C. This is illustrated by the finite element results discussed earlier in Fig. 2. For this relatively slender column ($L/R = 60$), $L_C = 0.05$ m, $L = 0.567$ m and $t_C = 0.00008$ s. The large buckling amplitudes evident in Fig. 2 are associated with $t/t_C > 5$, consistent with the analytical model. The imperfection wavelength giving rise to the largest buckle is roughly $1.5L_C$ (Fig. 5). On the other hand, the buckle wavelength for the less slender member with $L/R = 20$ which develops when $t/t_C \approx 3$ is close to L_C (Fig. 4). The relation between the fully developed buckle and the amplitude and shape of the initial imperfection under dynamic loading is complicated and in need of further elucidation.

The slight decrease after the initial peak in the maximum deflection for the case $L_I/L_C = 0.5$ in Fig. 11 is almost certainly associated with the neglect of elastic loading in the model. The discontinuity in slope of that response at $t/t_C \cong 1.5$ and subsequent increase is associated with the second local deflection peak from the end overtaking the magnitude of the first peak, as was mentioned in connection with Fig. 9.

6. Conclusions

Columns and plates loaded abruptly at one end such that an axial plastic wave is induced are stabilized by lateral inertia. Buckling deflections grow simultaneously with the axial compression wave propagating down the column from the loaded end.

Most importantly, before significant buckling deflections arise, the length of column subject to a given stress level can be three or more times greater than the length at which quasi-static buckling would take place. The importance of this phenomenon is that the column is able to dissipate all the plastic energy associated with the axial compression wave, as long as the column remains nearly straight. In the range of loading rates of interest here, much larger plastic strains occur due to the compressive axial wave than due to buckling. Thus, for slender members, the delay of buckling allows longer segments of the beam to experience the plastic strains due to the axial wave. If it is desired that the entire length of the member experience the full effect of the axial wave, then a the present results suggest the length should be roughly three times L_C as a rule of thumb, subject to the level of initial imperfection.

For columns or plates loaded with a uniform velocity V_0 at one end, the dimensionless parameter governing whether buckling and wave propagation are coupled is $V_0/c_0\varepsilon_Y$: if $V_0/c_0\varepsilon_Y > 5$, strong coupling occurs and bucklewaves are generated. The study in this paper has addressed nominally straight members loaded axially. The buckle wave phenomenon also occurs in straight members that are inclined to the faces of the sandwich plate such as columns in truss cores or plates in folded plate cores, as discussed by Vaughn et al. (2005). Although non-axial deformations occur immediately at the dynamically loaded end of the member where it is attached to the face, nevertheless, a well-developed axial wave is initiated and propagates along the member. Vaughn et al. (2005) showed that the phenomena discussed in Section 2 are also observed in inclined straight members. On the other hand, if the members are not nominally straight but have a significant bow, it is not likely that fully developed axial compression wave will occur, although this has not been investigated.

Acknowledgements

This work has been supported in part by the ONR under grant N00014-02-1-0700 and in part by the Division of Engineering and Applied Sciences, Harvard University.

References

ABAQUS/Explicit User's Manual, Ver. 6.2, 2001. Hibbit, Karlsson and Sorensen Inc.

Abrahamson, G.R., Goodier, J.N., 1966. Dynamic flexural buckling of rods within an axial plastic compression wave. J. Appl. Mech. 33, 241–247.

Anwen, W., Wenying, T., 2003. Characteristic-value analysis for plastic dynamic buckling of columns under elastoplastic compression waves. Int. J. Non-Linear Mech. 38, 615–628.

Ari-Gur, J., Weller, T., Singer, J., 1982. Experimental and theoretical studies of columns under axial impact. Int. J. Solids Structures 18, 619–641.

Bell, J.F., 1988. The dynamic buckling of rods at large plastic strain. Acta Mech. 74, 51–67.

Carrier, G.F., 1949. The spaghetti problem. Amer. Math. Monthly LVI (10), 669–672.

Fleck, N.A., Deshpande, V.S., 2004. The resistance of clamped sandwich beams to shock loading. J. Appl. Mech. 71, 386–401.

Hayashi, T., Sano, Y., 1972. Dynamic buckling of bars (2nd report, the case of high velocity impact). Bull. JSME 88, 1176–1184.

Hutchinson, J.W., Xue, Z., 2005. Metal sandwich plates optimized for pressure impulses. Int. J. Mech. Sci. 47, 545–569.

Jones, N., Reis, H., 1980. On the dynamic buckling of a simple elastic-plastic model. Int. J. Solids Structures 16, 969–989.

Karagiozova, D., Jones, N., 1996. Dynamic elastic-plastic buckling phenomena in a rod due to axial impact. Int. J. Impact Engrg. 18, 919–947.

Kenny, S., Pegg, N., Taheri, F., 2002. Finite element investigations on the dynamic plastic buckling of a slender beam subject to axial impact. Int. J. Impact Engrg. 27, 179–195.

Lepik, U., 2001. Dynamic buckling of elastic-plastic beams including effects of axial stress waves. Int. J. Impact Engrg. 25, 537–552.

Su, X.Y., Yu, T.X., Reid, S.R., 1995. Inertia-sensitive impact energy-absorbing structures, part 1: effects of inertia and elasticity. Int. J. Impact Engrg. 16, 651–672.

Taylor, G.I., 1958. The Scientific Papers of G.I. Taylor, vol. 1. Cambridge University Press, London.

Thornton, P.H., Yeung, K.S., 1990. The dynamic buckling of sheet steel. Int. J. Impact Engrg. 9, 379–388.

Vaughn, D.G., Canning, J.M., Hutchinson, J.W., 2005. Coupled plastic wave propagation and column buckling. J. Appl. Mech. 72, 139–146.

Von Karman, T., Duwez, P., 1950. The propagation of plastic deformation in solids. J. Appl. Phys. 21, 987–994.

Xue, Z., Hutchinson, J.W., 2004. A comparative study of impulse-resistant metallic sandwich plates. Int. J. Impact Engrg. 30, 1283–1305.